Letter

Renormalized quasiparticles, topological monopoles, and superconducting line nodes in heavy-fermion CeTX_3 compounds

Vsevolod Ivanov,[1,*] Xiangang Wan,[2] and Sergey Y. Savrasov[1,†]
[1]*Department of Physics, University of California, Davis, California 95616, USA*
[2]*Department of Physics, Nanjing University, Nanjing 210093, China*

(Received 27 July 2020; revised 23 November 2020; accepted 12 January 2021; published 25 January 2021)

Noncentrosymmetric superconductors have recently attracted much attention, since the lack of inversion symmetry mixes spin-singlet and -triplet pairing states, which may allow the realization of topological superconductivity. In this Letter, we study the electronic properties of the family of inversion-broken CeTX_3 heavy-fermion superconductors, finding topological nodal lines as well as Dirac and Weyl points, which are renormalized closer to the Fermi energy by correlations. We find that the Weyl nodal lines have a substantial effect on the Fermi surface spin structure of the normal state and lead to line nodes in the superconducting phase.

DOI: 10.1103/PhysRevB.103.L041112

Superconductivity (SC) in noncentrosymmetric compounds has received much attention due to their potential for hosting unconventional pairing states. The lack of inversion symmetry permits antisymmetric spin-orbit coupling (ASOC), which splits the Fermi surface (FS) and mixes spin-singlet and spin-triplet SC pairing states.

The CeTX_3 (T = Co, Rh, Ir, X = Si, Ge) family of compounds crystallize in the $BaNiSn_3$-type structure ($I4mm$ space group no. 107), which breaks spatial inversion symmetry. With the exception of paramagnetic $CeCoSi_3$, their low-temperature phases are antiferromagnetic (AF) at ambient pressure. Application of pressure suppresses the Néel temperature to zero, where the magnetic ground state gives way to SC. The SC in this group exhibits many unconventional features, including upper critical fields H_{c2} that far exceed the Pauli limiting field $H_p[T] \sim 1.86T_C[K]$ [1–8], which has been suggested as evidence of an odd parity SC gap function. Recent works argue that AF fluctuations play a role in the development of SC, indicating the importance of the spin structure to the unconventional physics in these compounds.

The absence of inversion symmetry is also a necessary ingredient for the existence of topological Weyl points (WPs). Since the role of ASOC and lack of inversion symmetry in the development of the SC state is not well understood, we hope to shed some light by investigating the topological properties of these materials. Furthermore, the narrow Ce-4f band is sensitive to temperature and pressure, allowing WPs to be tuned without introduction of chemical or site disorder. This feature makes these heavy-fermion materials promising candidates for the study of Weyl physics [9] in the proximity of SC and quantum criticality.

Our electronic-structure calculations are performed within the framework of the full potential linear muffintin orbital method with spin-orbit coupling, using the experimentally measured lattice parameters [10–13]. The compounds are locked to the paramagnetic state to mimic the experimentally observed suppression of magnetism by pressure. The on-site interactions between the Ce-4f electrons must be treated with special care, as the strong Coulomb repulsion narrows the bandwidth considerably. We handle renormalization of quasiparticle bands through the LDA + Gutzwiller (LDA + G) method, taking Hubbard U values of 5 eV and 6 eV [14]. The method is described in more detail in Refs. [15–19].

In LDA + G, the double-counting potential must carefully be chosen to account for the Coulomb correction included in both the single-particle and interacting terms of the Hamiltonian. Specifically, for the electron self-energy correction, $\Sigma_\alpha(0) - V_{\mathrm{DC},\alpha}$, there are several options for the double counting potential $V_{\mathrm{DC},\alpha}$ [15]. One such option is to set $V_{\mathrm{DC},\alpha} = \Sigma_\alpha(0)$, which leaves the LDA FS intact. Another option is to compute the crystal-field modifications self-consistently using an average over orbital self-energies, $V_{\mathrm{DC},\alpha} = \frac{1}{N}\sum_\alpha^N \Sigma_\alpha(0)$.

For the CeTX_3 compounds, the crystalline electric field (CEF) effect of the tetragonal symmetry lifts the degeneracy of the $J = 5/2$ total angular momentum state, splitting it into three doublets. Magnetic susceptibility and inelastic neutron scattering experiments [11,20–22] have determined the ground-state doublet to be $\Gamma_7^{(1)}$ with Γ_6 and $\Gamma_7^{(2)}$ slightly higher in energy. Our LDA calculation shows that the lowest energy doublet hybridizes with the four bands crossing the Fermi energy (E_F), which are largely responsible for the shape of the FS. This is consistent with prior works that show qualitative agreement between the LDA FS and experimental de Haas-van Alphen measurements for $CeRhSi_3$ [13]. To best match the experimentally determined FSs and mass enhancements, we take a phenomenological approach, selecting a hybrid double counting scheme which independently treats the lowest energy doublets while the remaining states are shifted upward by 0.1 Ry [23]. A different choice of shift parameter does not affect the states near the Fermi energy,

*vivanov@ucdavis.edu
†savrasov@physics.ucdavis.edu

TABLE I. Quasiparticle residues z_α for the lowest energy states for the members of the CeTX_3 series.

	$z_{\mathrm{LDA+G}}$ $(U = 5\,\mathrm{eV})$			$z_{\mathrm{LDA+G}}$ $(U = 6\,\mathrm{eV})$		
	$\Gamma_7^{(1)}$	Γ_6	$\Gamma_7^{(2)}$	$\Gamma_7^{(1)}$	Γ_6	$\Gamma_7^{(2)}$
$CeCoSi_3$	0.59	0.57	0.87	0.54	0.52	0.82
$CeRhSi_3$	0.43	0.41	0.86	0.37	0.36	0.81
$CeIrSi_3$	0.43	0.42	0.86	0.38	0.36	0.81
$CeCoGe_3$	0.38	0.36	0.85	0.33	0.32	0.78
$CeRhGe_3$	0.16	0.14	0.92	0.12	0.10	0.89
$CeIrGe_3$	0.15	0.14	0.93	0.11	0.09	0.91

and does not change the conclusions of our work. An analogous energy shift was used to find the FS of the isostructural LaTX_3, which is presumed to be very similar to that of the respective CeTX_3 compounds since their Ce-4f electrons are highly localized [24,25].

Our LDA + G procedure yields band-dependent quasiparticle residues z_α, which are summarized in Table I. It is worth noting that the $\Gamma_7^{(2)}$ doublet has been determined to be the lowest lying state in $CeRhSi_3$ [25]. However, our calculations place the $\Gamma_7^{(1)}$ doublet at the lowest energy for all six isoelectronic compounds.

The trends in the CeTX_3 series can be understood in terms of a Doniach phase diagram arising from competing RKKY and Kondo interactions [26]. The tuning parameter in the Doniach phase diagram is $|J_{cf}|N(0)$ where J_{cf} is the magnetic exchange interaction and $N(0)$ is the density of states at the E_F. Experimentally, this parameter can be tuned by compressing the lattice using pressure, resulting in a greater hybridization of the conduction and Ce-4f bands, thus decreasing the localization of the electrons. This is reflected directly in the trend of Néel temperatures, with $CeTGe_3$ compounds exceeding their Si counterparts, (T_N = 21 K, 14.6 K, 8.7 K vs 0K, 1.8 K, 5.0 K for T = Co, Rh, Ir), due to their larger lattice constants [10]. The Néel temperatures of $CeRhSi_3$ and $CeIrSi_3$ are suppressed to zero at relatively low pressures $P_c \sim 2$ GPa, indicating their proximity to a quantum critical point.

The computed z_α values follow a decreasing trend with increasing lattice volumes, and qualitatively match the experimental trend of larger quasiparticle masses as the mass of the transition metal atom increases. These imply a factor of ~2-ninefold increase in Sommerfield γ values, but experimental measurements on CeTX_3 compounds in the high-pressure paramagnetic state are not presently available for comparison.

The bands crossing E_F are predominantly Ce-4f in character, with a minor contribution from the transition metal d orbitals away from the Fermi level. When Coulomb interactions are considered through the LDA + G calculation described above, their bandwidth is narrowed and the Fermi level is pinned to the lower doublet due to the increased density of states (Fig. 1), changing the electronic structure and associated topological features near E_F. We emphasize that while the particular number and shape of the topological features depend on the choice of double counting potential and magnitude of Hubbard-U, their existence is guaranteed

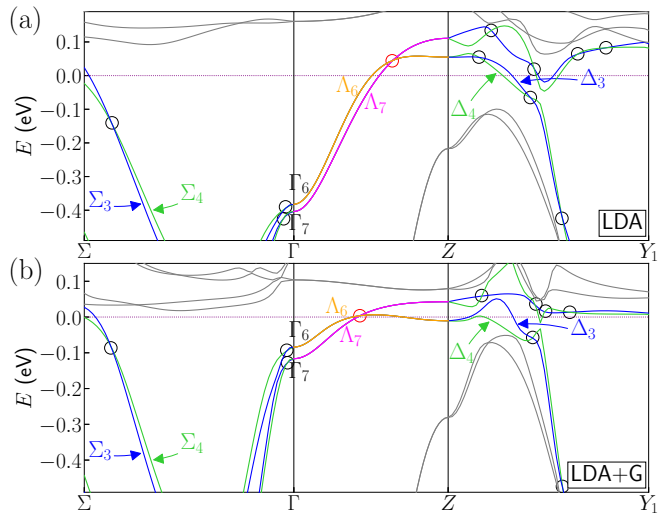

FIG. 1. Band structures for $CeCoGe_3$ using (a) LDA, and (b) LDA + G. Bands are labeled with their character representations according to their mirror eigenvalue: Σ_3/Δ_3 (blue) for -i and Σ_4/Δ_4 (green) for i within the mirror planes. Along the $\Gamma - Z$ line, doublets Λ_6 (orange) and Λ_7 (magenta) form a DP. NL crossings, and DPs are indicated by black and red circles, respectively.

by symmetry and robust to correlations. Since the CeTX_3 compounds are isoelectronic, the general picture of their topological properties is the same, with each compound hosting different sets of particular features based on the relative band positions determined by the CEF splitting. For the remainder of this work, we will focus on describing the electronic properties of $CeCoGe_3$, which hosts representative members of each type of topological features found in the series, including Dirac points (DPs) [27–32], WPs [33–36], and nodal lines (NLs) [37–40].

To locate and confirm the topological features, we use a one-shot method for data mining the bands [41]. We divide the Brillouin zone (BZ) into an initial $20 \times 20 \times 20$ **k** grid, computing the integral of Berry curvature fluxes through the surface of each **k** cube to find sources and sinks. The locations of these topological points are recursively refined by repeating the procedure on a $4 \times 4 \times 4$ grid within their **k** cube until the desired precision is achieved, thus resolving much finer details of the material topology.

We find two classes of WPs in $CeCoGe_3$. The first appears in sets of eight confined to the $k_z = 0$ plane, while the second comes in sets of 16 which are additionally separated in the k_z direction. Table II shows selected WPs of $CeCoGe_3$ listed along with their presumptive counterparts in LDA + G, which are shifted slightly in momentum space due to band renormalization. In total, $CeCoGe_3$ has seven (eight) nonequivalent WPs in LDA (LDA + G); additional details can be found in the Supplemental Material (SM) [23].

The most striking topological structure in the BZ is the set of NLs emerging from the DP in this material. The band inversion mechanism generating the DP along the $\Gamma - Z$ axis is similar to that responsible for the DP in the inversion broken Cd_3As_2 [29], which shares the C_{4v} point group symmetry. Along the $\Gamma - Z$ direction, compatibility relations for

TABLE II. Nonequivalent WPs of $CeCoGe_3$, with columns: Topological charge (C), number of symmetry equivalent WP in this set (No.), location ($\mathbf{k}_{\mathrm{Weyl}}$) given in units of $(2\pi/a, 2\pi/a, 2\pi/c)$, and energy in meV (E). The Fermi energy is set to 0 eV.

$CeCoGe_3$		LDA		LDA+G	
C	#	$\mathbf{k}_{\mathrm{Weyl}}$	E	$\mathbf{k}_{\mathrm{Weyl}}$	E
+1	8	(0.097, 0.187, 1.000)	−109	(0.161, 0.133, 1.000)	−49
−1	16	(0.118, 0.152, 0.556)	−140	(0.131, 0.168, 0.586)	−110
+1	16	(0.235, 0.271, 0.676)	+78	(0.167, 0.236, 0.530)	+33
−1	16	(0.057, 0.285, 0.996)	+118	(0.083, 0.221, 0.617)	+37

the double group connect $\Gamma_7 \to \Lambda_7$ and $\Gamma_6 \to \Lambda_6$. When moving along $\Gamma - Z$, the lowest lying Λ_7 Kramer's doublet switches with the Λ_6 doublet. The DP formed by the two doublets persists with the inclusion of band renormalizations, shifting from a position $k_z = 0.644\frac{2\pi}{c}$ in LDA to $k_z = 0.4285\frac{2\pi}{c}$ in LDA + G, closer to the Γ point, as shown in Fig. 1.

Moving away from the $\Gamma - Z$ axis within the σ_v (σ_d) mirror plane, compatibility relations dictate that the Λ_6 and Λ_7 doublets split into bands with Σ_3/Σ_4 (Δ_3/Δ_4) irreducible representation. They can be distinguished by their mirror eigenvalue, with $-i$ corresponding to Σ_3/Δ_3 and $+i$ to Σ_4/Δ_4. Intersecting bands belonging to different mirror plane irreducible representations form a topologically protected continuous line of degeneracy called a Weyl NL [42]. Such NLs are protected by mirror symmetry, and are robust against perturbations. Verification of NL topology is further discussed in the SM [23].

A selection of NLs in $CeCoGe_3$ are shown in Fig. 2. In LDA, three NLs emerge from the DP, with NL-2 and NL-3 forming loops within the σ_v plane and NL-4 forming a loop in the σ_d planes. The two other NLs within the σ_d plane, NL-1 and NL-5, do not form loops, instead connecting across the edge of the BZ. When correlations are considered, the NL structure of $CeCoGe_3$ changes dramatically. NL-3 mixes with other NLs (not pictured), inverting to connect across the $k_z = 0$ plane, nearly coinciding with NL-2, while NL-4 and NL-5 are destroyed by correlations. On the other hand, the momentum-space structures of NL-1 and NL-2 do not change much in LDA + G. We note that since NL-3 and NL-4 are very small features and are strongly affected by correlations, it is unlikely that they can be resolved experimentally. The SM [23] contains the details of several additional NLs which lie farther from E_F, for a total of 15 (12) NLs in LDA (LDA + G).

As we have mentioned previously, the renormalization of quasiparticle bands by correlations affects not only the momentum-space position of topological features, but also the energy at which they are located. Coulomb interactions substantially reduce the width of the Ce-4f bands and pin them to the Fermi energy due to the increased density of states. A consequence of this renormalization is that any topological features formed by the Ce-4f bands move closer to the E_F, becoming more relevant for the SC physics.

We illustrate this by showing the renormalization of the first WP in Table II as well as NL-1 and NL-2 (Fig. 3). Since the two NLs are formed from bands with a large Ce-4f component, the renormalization of these bands by correlations has a twofold effect, narrowing the energy dispersion of the NLs and move them closer to the E_F. Likewise, the WP located at $(0.09700\frac{2\pi}{a}, 0.18704\frac{2\pi}{a}, 1.0\frac{2\pi}{c})$ is formed from bands that have primarily Ce-4f character near this momentum. The correlations introduced by LDA + G raise the energy by 60 meV, and shift the WP to a new momentum space position $(0.16138\frac{2\pi}{a}, 0.13255\frac{2\pi}{a}, 1.0\frac{2\pi}{c})$.

While SC in the $CeTX_3$ compounds has been studied extensively, the nature of the pairing state has not been settled. There are a number of good reviews on SC in noncentrosymmetric materials [43–46], which we will briefly outline here. The absence of inversion symmetry allows for an ASOC term,

$$H_{\mathrm{ASOC}} = \sum_{\mathbf{k}} \sum_{\alpha\beta=\uparrow,\downarrow} \boldsymbol{\gamma}(\mathbf{k}) \cdot \tilde{\boldsymbol{\sigma}}_{\alpha\beta} c^{\dagger}_{\mathbf{k}\alpha} c_{\mathbf{k}\beta}, \tag{1}$$

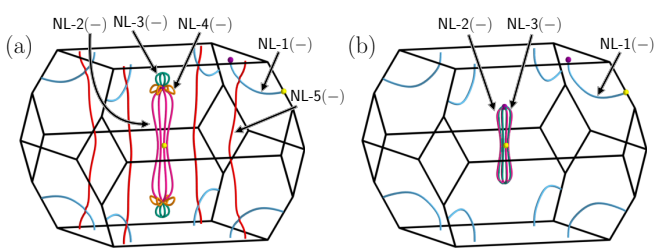

FIG. 2. Selected NLs in $CeCoGe_3$ for LDA (a), and LDA + G (b), with colored spheres showing start (yellow)/end (purple) points for NLs plotted in Fig. 3.

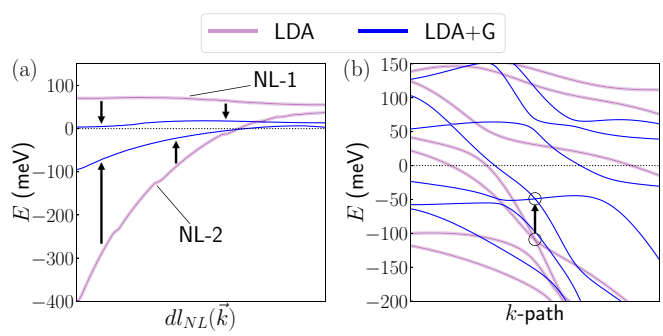

FIG. 3. Renormalization of topological features in $CeCoGe_3$ between LDA (violet) and LDA + G (blue). (a) Renormalization of NL-1 and NL-2. Energy is plotted along the length of each NL (normalized to unity), with start/end points as shown in Fig. 2. (b) Plots of bands around the first WP from Table II. k-path is the straight line connecting $\mathbf{k}_{\mathrm{Weyl}} \pm 0.1\hat{k}_y$.

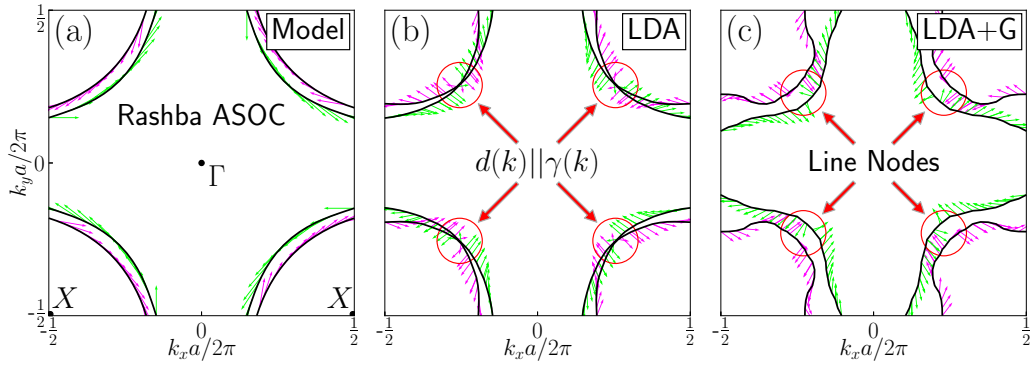

FIG. 4. Plots of the FS of $CeCoGe_3$ within the $k_z = 0$ plane for (a) the TB model, (b) LDA, and (c) LDA + G. Green (magenta) arrows show the direction of spins projected into the $xy-$ plane for the upper (lower) band at each point. For LDA + G, the energy is shifted by -5 meV to avoid FS distortion due to pockets created by a set of type-II WPs located just above E_f. Red circles highlight the spin distortion caused by the NLs in the normal state, which indicates the existence of zeros in $\boldsymbol{\gamma}(\mathbf{k})$ and implies line nodes in the SC gap function.

where the Pauli matrices $\tilde{\boldsymbol{\sigma}} = (\tilde{\sigma}_x, \tilde{\sigma}_y, \tilde{\sigma}_z)$ act on the pseudospin basis states $|\mathbf{k}, \uparrow\rangle$ and $|\mathbf{k}, \downarrow\rangle$, and $c^\dagger_{\mathbf{k}\alpha}(c_{\mathbf{k}\beta})$ are the corresponding creation (annihilation) operators.

The form of $\boldsymbol{\gamma}(\mathbf{k})$ explicitly determines the local spin structure in $\mathbf{k}$ space. This places a constraint on the superconducting gap function $\Delta(k)$, which in general can be expanded in the basis of Pauli matrices as $\Delta(k) = [\psi(\mathbf{k}) + \mathbf{d}(\mathbf{k}) \cdot \tilde{\boldsymbol{\sigma}}]i\tilde{\sigma}_y$, with even-parity scalar $\psi(k)$ (singlet) and odd-parity vector $\mathbf{d}(\mathbf{k})$ (triplet) components. For sufficiently strong ASOC, $|\pm\mathbf{k}, \uparrow\rangle$ states become nondegenerate, which suppresses the component of $\mathbf{d}(\mathbf{k})$ that is not parallel to $\boldsymbol{\gamma}(\mathbf{k})$ [43,44,47,48]. It then follows that the triplet component of the gap $\mathbf{d}(\mathbf{k})$ can be inferred directly from the spin structure at the FS. The symmetry of the pairing gap has been studied in the context of AFM spin fluctuations near the SC transition [49,50]. It has also been suggested that $CeRhSi_3$ and $CeIrSi_3$ may be topological Weyl superconductors [51,52], and indeed our present study has identified a number Weyl nodes in the energy dispersion. However, the WPs found in our calculations are type II, with a hyperbolic FS that does not enclose the node. Their contribution to the FS topology is quite small, and most are too far away from E_f to be relevant for the SC physics, even when taking band renormalization into account.

Instead, we focus on the effect of topological NLs found in these compounds, which occupy a significantly larger phase space. Figure 4 shows cross sections of the $CeCoGe_3$ FS in the $k_z = 0$ plane for LDA and LDA + G, compared to a two-band (TB) model [Fig. 4(a)] which reproduces the principal FS features of the $CeTX_3$ family [49], showing a realignment of the spins beyond the usual Rashba-type ASOC due to the topological NLs near E_F. In LDA, the type-II NL NL-5 passes through the $k_x k_y$ plane close to E_F, and its strongly tilted dispersion results in hyperboloid FS sheets around the X point in Fig. 4(b). The spins along the surface rotate by an angle π in the vicinity of the NL, creating a vortexlike defect which shrinks as the energy approaches the NL intersection. Exactly at the NL energy, this vortex becomes vanishingly small but the spin texture remains continuous due to the degeneracy of the bands. An animation of the spin rotations resulting from the NLs is included in the SM [23]. In LDA + G [Fig. 4(c)], correlations shift the NL away from E_F, resulting in a gap between the FSs, but leave the vortexlike spin defect unaffected. This spin distortion at the σ_d planes is a direct consequence of the topological nature of the NLs, making it distinct from spin structures beyond Rashba ASOC which have been considered in other works [53–55].

It has been proposed that line nodes in the superconducting gap function could arise as a result of a topological defect in $\boldsymbol{\gamma}(\mathbf{k})$, and that such a state would be dominated by spin-triplet pairing and robust to perturbation [56]. The vortexlike defects in the spin structure that arise from the topological NLs in the normal state of $CeTX_3$ compounds can therefore serve as a natural origin for line nodes in the superconducting gap. This result is consistent with experiments that have found evidence of gapless line-node SC in $CeRhSi_3$ and $CeIrSi_3$ [8,57–59]. Additional experiments are needed to clarify the form of the SC gap in this family of materials.

In summary, we have performed simulations of SC compounds in the $CeTX_3$ series with LDA and LDA + G, choosing the double counting potential in such a way that reproduces the experimental FSs. We characterized the topological properties of their energy dispersion finding WPs and NLs, which are renormalized close to the E_F by the strong Coulomb interactions of the $Ce-4f$ orbitals. These topological features in turn affect the spin structure at the FS in these materials, which we have used to make a first-principles prediction of the superconducting gap structure.

This work was supported by NSF DMR Grant No. 1832728. X.G.W. acknowledges support from NSFC 11834006 and the Tencent Foundation through the XPLORER PRIZE.

[1] R. Settai, Y. Okuda, I. Sugitani, Y. nuki, T. D. Matsuda, Y. Haga, and H. Harima, Int. J. Mod. Phys. B **21**, 3238 (2007).

[2] N. Kimura, K. Ito, K. Saitoh, Y. Umeda, H. Aoki, and T. Terashima, Phys. Rev. Lett. **95**, 247004 (2005).

[3] F. Honda, I. Bonalde, K. Shimizu, S. Yoshiuchi, Y. Hirose, T. Nakamura, R. Settai, and Y. Ōnuki, Phys. Rev. B **81**, 140507(R) (2010).

[4] I. Sugitani, Y. Okuda, H. Shishido, T. Yamada, A. Thamizhavel, E. Yamamoto, T. D. Matsuda, Y. Haga, T. Takeuchi, R. Settai, and Y. nuki, J. Phys. Soc. Jpn. **75**, 043703 (2006).

[5] H. Wang, J. Guo, E. D. Bauer, V. A. Sidorov, H. Zhao, J. Zhang, Y. Zhou, Z. Wang, S. Cai, K. Yang, A. Li, X. Li, Y. Li, P. Sun, Y.-f. Yang, Q. Wu, T. Xiang, J. D. Thompson, and L. Sun, Phys. Rev. B **97**, 064514 (2018).

[6] T. Kawai, M. Nakashima, Y. Okuda, H. Shishido, T. Shimoda, T. D. Matsuda, Y. Haga, T. Takeuchi, M. Hedo, Y. Uwatoko, R. Settai, and Y. nuki, J. Phys. Soc. Jpn. **76**, 166 (2007).

[7] R. Settai, Y. Miyauchi, T. Takeuchi, F. Lvy, I. Sheikin, and Y. nuki, J. Phys. Soc. Jpn. **77**, 073705 (2008).

[8] N. Kimura, K. Ito, H. Aoki, S. Uji, and T. Terashima, Phys. Rev. Lett. **98**, 197001 (2007).

[9] H.-H. Lai, S. E. Grefe, S. Paschen, and Q. Si, Proc. Natl. Acad. Sci. USA **115**, 93 (2018).

[10] T. Kawai, H. Muranaka, M.-A. Measson, T. Shimoda, Y. Doi, T. D. Matsuda, Y. Haga, G. Knebel, G. Lapertot, D. Aoki, J. Flouquet, T. Takeuchi, R. Settai, and Y. nuki, J. Phys. Soc. Jpn. **77**, 064716 (2008).

[11] A. D. Hillier, D. T. Adroja, P. Manuel, V. K. Anand, J. W. Taylor, K. A. McEwen, B. D. Rainford, and M. M. Koza, Phys. Rev. B **85**, 134405 (2012).

[12] V. K. Pecharsky, O.-B. Hyun, and K. A. Gschneidner, Phys. Rev. B **47**, 11839 (1993).

[13] T. Terashima, M. Kimata, S. Uji, T. Sugawara, N. Kimura, H. Aoki, and H. Harima, Phys. Rev. B **78**, 205107 (2008).

[14] B. T. Thole, G. van der Laan, J. C. Fuggle, G. A. Sawatzky, R. C. Karnatak, and J.-M. Esteva, Phys. Rev. B **32**, 5107 (1985).

[15] R. Dong, X. Wan, X. Dai, and S. Y. Savrasov, Phys. Rev. B **89**, 165122 (2014).

[16] Y. X. Yao, C. Z. Wang, and K. M. Ho, Phys. Rev. B **83**, 245139 (2011).

[17] K. M. Ho, J. Schmalian, and C. Z. Wang, Phys. Rev. B **77**, 073101 (2008).

[18] X. Deng, X. Dai, and Z. Fang, Europhys. Lett. **83**, 37008 (2008).

[19] X. Deng, L. Wang, X. Dai, and Z. Fang, Phys. Rev. B **79**, 075114 (2009).

[20] Y. Okuda, Y. Miyauchi, Y. Ida, Y. Takeda, C. Tonohiro, Y. Oduchi, T. Yamada, N. Duc Dung, T. D. Matsuda, Y. Haga, T. Takeuchi, M. Hagiwara, K. Kindo, H. Harima, K. Sugiyama, R. Settai, and Y. nuki, J. Phys. Soc. Jpn. **76**, 044708 (2007).

[21] M. Smidman, D. T. Adroja, A. D. Hillier, L. C. Chapon, J. W. Taylor, V. K. Anand, R. P. Singh, M. R. Lees, E. A. Goremychkin, M. M. Koza, V. V. Krishnamurthy, D. M. Paul, and G. Balakrishnan, Phys. Rev. B **88**, 134416 (2013).

[22] V. K. Anand, A. D. Hillier, D. T. Adroja, D. D. Khalyavin, P. Manuel, G. Andre, S. Rols, and M. M. Koza, Phys. Rev. B **97**, 184422 (2018).

[23] See Supplemental Material at http://link.aps.org/supplemental/10.1103/PhysRevB.103.L041112 for more calculation details and a video showing spin rotations near the topological nodal lines.

[24] A. Thamizhavel, H. Shishido, Y. Okuda, H. Harima, T. D. Matsuda, Y. Haga, R. Settai, and Y. nuki, J. Phys. Soc. Jpn. **75**, 044711 (2006).

[25] Y. Muro, M. Ishikawa, K. Hirota, Z. Hiroi, N. Takeda, N. Kimura, and H. Aoki, J. Phys. Soc. Jpn. **76**, 033706 (2007).

[26] S. Doniach, Phase diagram for the Kondo lattice, in *Valence Instabilities and Related Narrow-Band Phenomena*, edited by R. D. Parks (Springer US, Boston, MA, 1977), pp. 169–176.

[27] S. M. Young, S. Zaheer, J. C. Y. Teo, C. L. Kane, E. J. Mele, and A. M. Rappe, Phys. Rev. Lett. **108**, 140405 (2012).

[28] Z. Wang, Y. Sun, X.-Q. Chen, C. Franchini, G. Xu, H. Weng, X. Dai, and Z. Fang, Phys. Rev. B **85**, 195320 (2012).

[29] Z. Wang, H. Weng, Q. Wu, X. Dai, and Z. Fang, Phys. Rev. B **88**, 125427 (2013).

[30] B.-J. Yang and N. Nagaosa, Nat. Commun. **5**, 4898 (2014).

[31] Q. D. Gibson, L. M. Schoop, L. Muechler, L. S. Xie, M. Hirschberger, N. P. Ong, R. Car, and R. J. Cava, Phys. Rev. B **91**, 205128 (2015).

[32] Y. Du, B. Wan, D. Wang, L. Sheng, C.-G. Duan, and X. Wan, Sci. Rep. **5**, 14423 (2015).

[33] X. Wan, A. M. Turner, A. Vishwanath, and S. Y. Savrasov, Phys. Rev. B **83**, 205101 (2011).

[34] H. Weng, C. Fang, Z. Fang, B. A. Bernevig, and X. Dai, Phys. Rev. X **5**, 011029 (2015).

[35] S.-M. Huang, S.-Y. Xu, I. Belopolski, C.-C. Lee, G. Chang, B. Wang, N. Alidoust, G. Bian, M. Neupane, C. Zhang, S. Jia, A. Bansil, H. Lin, and M. Z. Hasan, Nat. Commun. **6**, 7373 (2015).

[36] A. A. Soluyanov, D. Gresch, Z. Wang, Q. Wu, M. Troyer, X. Dai, and B. A. Bernevig, Nature **527**, 495 (2015).

[37] A. A. Burkov, M. D. Hook, and L. Balents, Phys. Rev. B **84**, 235126 (2011).

[38] R. Yu, H. Weng, Z. Fang, X. Dai, and X. Hu, Phys. Rev. Lett. **115**, 036807 (2015).

[39] Y. Kim, B. J. Wieder, C. L. Kane, and A. M. Rappe, Phys. Rev. Lett. **115**, 036806 (2015).

[40] Y. Du, F. Tang, D. Wang, L. Sheng, E.-j. Kan, C.-G. Duan, S. Y. Savrasov, and X. Wan, npj Quantum Mater. **2**, 3 (2017).

[41] V. Ivanov and S. Y. Savrasov, Phys. Rev. B **99**, 125124 (2019).

[42] C. Fang, H. Weng, X. Dai, and Z. Fang, Chin. Phys. B **25**, 117106 (2016).

[43] E. Bauer and M. Sigrist, *Non-Centrosymmetric Superconductors* (Springer, Berlin, 2012).

[44] M. Smidman, M. B. Salamon, H. Q. Yuan, and D. F. Agterberg, Rep. Prog. Phys. **80**, 036501 (2017).

[45] S. Yip, Annu. Rev. Condens. Matter Phys. **5**, 15 (2014).

[46] F. Kneidinger, E. Bauer, I. Zeiringer, P. Rogl, C. Blaas-Schenner, D. Reith, and R. Podloucky, Special issue of Superconducting Materials: Conventional, Unconventional and Undetermined, Physica C **514**, 388 (2015).

[47] P. A. Frigeri, D. F. Agterberg, A. Koga, and M. Sigrist, Phys. Rev. Lett. **92**, 097001 (2004).

[48] K. V. Samokhin and V. P. Mineev, Phys. Rev. B **77**, 104520 (2008).

[49] Y. Tada, N. Kawakami, and S. Fujimoto, J. Phys. Soc. Jpn. **77**, 054707 (2008).

[50] Y. Tada, N. Kawakami, and S. Fujimoto, Phys. Rev. B **81**, 104506 (2010).

[51] A. Daido and Y. Yanase, Phys. Rev. B **94**, 054519 (2016).

[52] T. Yoshida and Y. Yanase, Phys. Rev. B **93**, 054504 (2016).

[53] Z. Zhong, A. Tóth, and K. Held, Phys. Rev. B **87**, 161102(R) (2013).

[54] D. Y. Usachov, I. A. Nechaev, G. Poelchen, M. Güttler, E. E. Krasovskii, S. Schulz, A. Generalov, K. Kliemt, A. Kraiker, C.

Krellner, K. Kummer, S. Danzenbächer, C. Laubschat, A. P. Weber, J. Sánchez-Barriga, E. V. Chulkov, A. F. Santander-Syro, T. Imai, K. Miyamoto, T. Okuda, and D. V. Vyalikh, Phys. Rev. Lett. **124**, 237202 (2020).

[55] R. Moriya, K. Sawano, Y. Hoshi, S. Masubuchi, Y. Shiraki, A. Wild, C. Neumann, G. Abstreiter, D. Bougeard, T. Koga, and T. Machida, Phys. Rev. Lett. **113**, 086601 (2014).

[56] Y. Yanase and M. Sigrist, J. Phys. Soc. Jpn. **77**, 124711 (2008).

[57] H. Mukuda, T. Fujii, T. Ohara, A. Harada, M. Yashima, Y. Kitaoka, Y. Okuda, R. Settai, and Y. Onuki, Phys. Rev. Lett. **100**, 107003 (2008).

[58] H. Mukuda, T. Ohara, M. Yashima, Y. Kitaoka, R. Settai, Y. Ōnuki, K. M. Itoh, and E. E. Haller, Phys. Rev. Lett. **104**, 017002 (2010).

[59] J. F. Landaeta, D. Subero, D. Catalá, S. V. Taylor, N. Kimura, R. Settai, Y. Ōnuki, M. Sigrist, and I. Bonalde, Phys. Rev. B **97**, 104513 (2018).